scientific reports

Check for updates

OPEN

Epoxy-based nanocomposites containing sustainable fillers for the realization of speckle patterns for digital image correlation analysis

Michele Perrella[1]✉, Aurelio Bifulco[1], Antonio Aronne[1], Claudio Imparato[1], Immacolata Climaco[1], Mattia Bartoli[2,3], Matteo Bruno[1,5], Gabriele Cricrì[4] & Enrico Armentani[1]

The Digital Image Correlation (DIC) is a non-contact technique that analyses a sequence of images providing full field measurement of displacements and strains over time. The DIC experimental set-up requires a speckle pattern. In this work a new epoxy-based nanocomposite, containing TiO_2 nanoparticles and coffee-derived biochar fillers, was developed to obtain an ecofriendly flame-retardant material with suitable mechanical and optical properties for its use as speckle pattern for DIC applications. The optimized formulation is characterized by a uniform distribution of TiO_2 and biochar particles and can be employed as self-standing material during the manufacturing of composite reinforcements. The physicochemical properties, mechanical behaviour and fire performances of the nanocomposite are described. The incorporation of the additives in the epoxy resin increases the Young's modulus by around 30% and almost doubles the burn-through time with respect to pristine resin, suggesting a slight condensed phase mechanism arising from the synergistic action of TiO_2 and biochar. The effectiveness for creating DIC speckle patterns is validated by comparing the experimental strains measured by means of DIC analysis with those obtained through a traditional technique. Finally, the durability of the speckle patterns was assessed by accelerated thermal aging tests, confirming the potential application of the material in structural health monitoring of composite structures.

Keywords Epoxy resin nanocomposite, Digital image correlation, Experimental mechanics, Speckle pattern, Coffee biochar, Flammability

Digital Image Correlation (DIC) is an optical technique based on surface pattern recognition[1]. It allows the measurement of displacement and deformation fields of a structural element on the base of the computerized correlation of subsequent images of the monitored surface. If the deformation field to be acquired is in plane, a vision system with a single camera can be used to perform two-dimensional (2D) DIC analysis. Instead, the out of plane displacement fields of complex objects can be evaluated by means of three-dimensional (3D) DIC, using a stereoscopic vision system composed of two or more cameras[2].

DIC technique can be proficiency used in different engineering sectors, such as in structural health monitoring of aircraft components like wings under different load conditions during flight[3], in monitoring civil structures like bridges, often using optical targets[4,5], in recording gravity pipes deflection[6], and in dynamic analysis of complex composite marine structures[7]. Moreover, the behaviour of adhesively bonded composite repairs can be monitored through DIC full-field strain measurements. Information on damage propagation and corresponding

[1]Department of Chemical, Materials and Production Engineering, Università di Napoli Federico II, Piazzale Tecchio 80, Naples 80125, Italy. [2]Center for Sustainable Future Technologies—CSFT@POLITO, Via Livorno 60, Turin 10144, Italy. [3]Department of Applied Science and Technology, Politecnico di Torino, C.so Duca degli Abruzzi 24, Turin 10129, Italy. [4]Department of Industrial Engineering, Università di Napoli Federico II, Piazzale Tecchio 80, Naples 80125, Italy. [5]Present address: INFN Sezione di Napoli, National Institute for Nuclear Physics, via Cintia, Naples 80126, Italy. ✉email: michele.perrella@unina.it

structural integrity of strengthened structures with fibre-reinforced polymers (FRPs) can be also gathered from DIC analysis outputs[8,9].

DIC algorithms are based on the tracking of a recognizable pattern on the investigated surface in a sequence of images. The pattern is typically obtained through the application of paint, inks and dyes, powder particles[10,11], soft-thermal nanoimprint lithography[12]or laser engraving[13]. The main advantage of painted speckle pattern is the ease of realization and reduced time and cost for its realization. On the other hand, the surface applied pattern (i.e., paint and inks), well consolidated in laboratories DIC procedures[8], can be affected by environmental agents, variable thermal conditions, and ageing degradation in the in-situ applications. Thus, a durable pattern integrated within the monitored structure material represents a rewarding feature. In this context, the dispersion of particles and nanoparticles within a polymeric matrix appears to be a suitable solution for the manufacturing of composites including high-quality speckle patterns, as it allows to overcome all problems related to the adhesion between the speckle layer and substrate[14]. Due to their peculiar properties, epoxy resins are suitable for the production of both paints and reinforced composites with good mechanical properties[10,15–17]. The addition of inorganic nanoparticles (e.g. silica, titanium oxide) can modify mechanical performances of base epoxy material[18,19], and also improve the flame retardancy of polymer-based products. Indeed, the high flammability of polymers limits their application in several industrial fields as well as civil engineering and requires the use of flame retardant additives, which often include harmful compounds (e.g., halogenated organics) or critical raw materials (e.g., phosphorus). Biowastes have also been recently employed to enhance the fire response of epoxy resins and their nanocomposites[20]. Particularly, converting spent coffee grounds into a biochar improves the dispersion of the filler in the polymer matrix and its chemical and thermal stability[21]. In view of developing advanced solutions for deformation monitoring, the application of metal oxides and biochar in epoxy resins to give DIC speckle patterns and satisfactory overall performances still lacks in the literature.

In the present work, an epoxy-based nanocomposite was engineered with the purpose of integrating a suitable speckle pattern within the material to be used for DIC analysis. The nanocomposite was obtained by dispersing biochar derived from spent coffee grounds and titanium oxide (TiO_2) nanoparticles in an epoxy resin. Coffee grounds represent a largely produced biowaste (about 6 million tons per year[22]), while TiO_2 is a widely available and inexpensive material with high refractive index, commonly used as white pigment. The two additives play a double role: the black biochar particles and white TiO_2 nanoparticles generate a pattern with high optical contrast and both contribute to the improvement of thermal behaviour of the final product. The material was comprehensively characterized, from a physicochemical point of view, through spectroscopic and thermal analyses, as well as concerning the surface flammability. Moreover, quasi-static mechanical characterization was performed under flexural and tensile loading conditions. Strain response acquired by strain gauges during traction tests was compared with that obtained through DIC technique to confirm the pattern recognition effectiveness and accuracy. Finally, the analysis of the durability of the proposed nanocomposite was assessed by accelerated ageing tests.

Materials and methods

The epoxy-based nanocomposite was prepared by reusing an organic waste composed of biochar particles with different sizes that are volumetrically randomly distributed. Biochar particles and their aggregates, visible on the surfaces of the product, can be assimilated to a speckle pattern to be used for analyses based on the DIC technique. To improve the optical contrast between the polymer matrix and the biochar, TiO_2 nanoparticles were uniformly dispersed into the epoxy system to obtain a white background. The so prepared epoxy formulation may be used as matrix in FRP composite materials for structural repair applications, being applied in environments that require fire safety characteristics. Therefore, in addition to the chemical and mechanical characterizations, its flammability was analysed.

Materials

The biochar (BC) samples obtained by pyrolysis of spent coffee grounds (Arabica mixture), collected with permission from Katia Cafè (Turin, Italy) and supplied by Casa del Caffè Vergnano S.p.A. (Turin, Italy), and dried at 105 °C for 72 h in a ventilated oven. BC was produced by pyrolysis in a tubular furnace (Carbolite TZF 12/65/550, Neuhausen, Germany) by using nitrogen atmosphere (40 mL/min) using a heating rate of 10 °C/min for reaching 500 °C and keeping the systems at the final temperature for 30 min. BC was used without any additional purification. The average particle size of BC was about 100 µm and further reduced by 2 h ball milling (carried out in a 700 cm^3 Turbula T-2 C mixer (Willy A. Bachofen AG, Muttenz, Switzerland)) equipped with eight zirconium balls. A two-component epoxy resin system (SX10) made of diglycidyl ether of bisphenol-A (DGEBA) resin and isophorone diamine (IDA), a cycloaliphatic diamine hardener, purchased from MATES S.r.l. (Milan, Italy), was employed. Titanium dioxide (AEROXIDE TiO_2 P90) nanoparticles with average size of ~14 nm were acquired from Evonik (Hanau-Wolfgang, Germany). According to the manufacturer, the main crystalline phase of TiO_2 P90 nanoparticles is anatase and their specific surface area is between 70 and 110 m^2/g.

Synthesis of epoxy nanocomposites

The preparation of epoxy nanocomposites containing coffee biochar and titanium dioxide is reported in the following and Fig. 1 displays the main steps of the fabrication procedure. The formulations were prepared via one-pot methodology by adding and mixing DGEBA resin with IDA (26 wt% of the epoxy) and varying amounts of TiO_2 (from 1.5 to 2.9 wt%) and BC (from 0.6 to 1.7 wt%). Specifically, TiO_2 nanoparticles and BC were subsequently introduced into DGEBA and the suspension was stirred manually, with the aid of a vortex stirrer for about 1 min. Then, the hardener was added, and the mixture was stirred again, ensuring a good dispersion of the fillers. The formulations were poured into silicone rubber moulds, cured overnight (~ 12 h) at 60 °C and post-cured 4 h at 80 °C. The resulting self-standing composite materials showed a random pattern of black

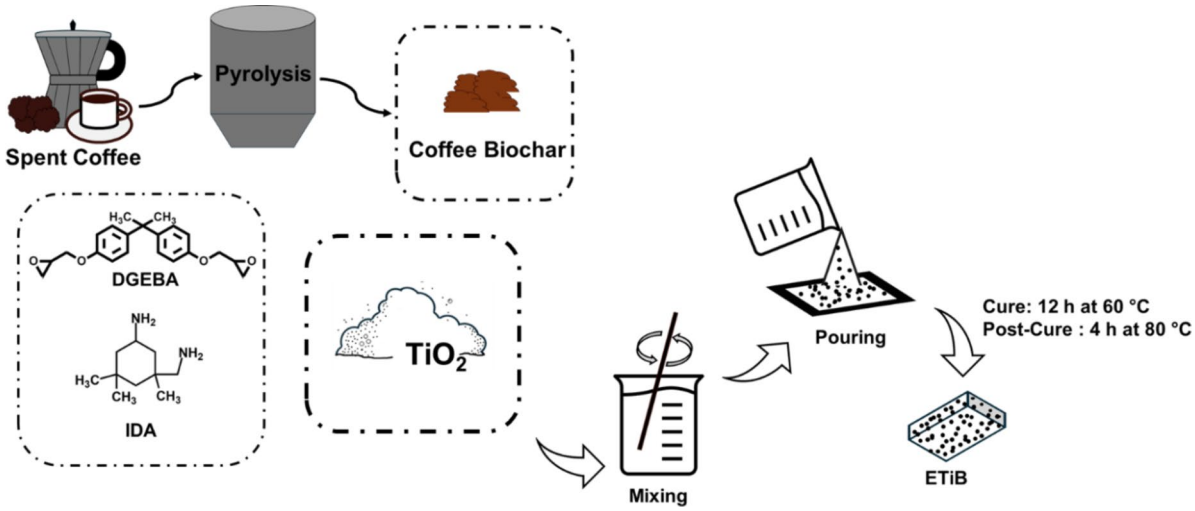

Fig. 1. One-pot fabrication of epoxy nanocomposites containing TiO_2 and coffee biochar.

spots on the surface, given by the exposed BC particles and their aggregates. These samples were characterized as described in the following. The optimized formulation, referred to as ETiB, contains 1.7 wt% BC and 2.9 wt% TiO_2 (with respect to the sum of DGEBA and IDA). The composition was determined on the basis of speckle pattern quality parameters, as reported below (Sect. Speckle pattern validation and Identification of the optimal composition for DIC patterns). To test the workability of the final product to be also used as paint, the formulation was, moreover, deposited onto different substrates by brush coating. Patterns comparable to those generated on the surface of self-standing composites were observed on the coatings.

Physicochemical characterization

Biochar samples were analysed by Raman spectroscopy using a Renishaw inVia (H43662model, Gloucestershire, UK) equipped with a laser line with a wavelength of 514 nm. Raman spectra were collected in the range from 500 cm^{-1} to 3500 cm^{-1} and the region between 1000 and 2000 cm^{-1} was analysed with a homemade software compiled in Matlab® (version R2020a) following a procedure reported by Tagliaferro et al.[23].

The morphology of biochar was investigated by using a field-emission scanning electron microscope (FE-SEM, Zeiss SupraTM40, Oberkochen, Germany) equipped with an energy-dispersive X-ray detector (EDX, Oxford Inca Energy 450, Oberkochen, Germany) for the evaluation of biochar elemental composition.

Particle size distribution of biochar was evaluated using a laser granulometry (FritschAnalysette 22, Idar-Oberstein, Germany) after a dispersion in ethanol and sonication in an ultrasonic bath for 10 min.

Fourier-transform infrared (FTIR) spectroscopy was carried out by means of a Nicolet 5700 FT spectrometer (Thermo Fisher, Waltham, MA) to confirm both the chemical composition and the completeness of the curing procedure. The spectra were recorded using a Thermo Scientific OMNIC Software Suite with 32 scans and a resolution of 4 cm^{-1}.

Thermogravimetric analysis (TGA) was performed to study the thermal behaviour of the unmodified cured resin and its nanocomposite. TA Instrument simultaneous thermoanalyser SDT Q600 under N_2 and air with a flow of 50 mL/min, and in the temperature range from 25 to 800 °C with a heating rate of 10 °C/min was employed. Differential scanning calorimetry (DSC) profiles were collected using the same apparatus in the temperature range from 25 to 200 °C with a heating rate of 10 °C/min. The glass transition temperature (Tg) was determined by the application of the tangent method to the second heating curve.

Burn-through tests were performed on pristine resin and epoxy nanocomposite to evaluate their burn-through resistance toward the application of a flame to the front side. A small-scale butane burner apparatus (Cadrim, China) was used to carry out the test. The flame temperature was about 1200 °C and the generated front heat flux was around 170 kW/m^2. The back-side temperatures of two sets of three specimens ($10 \times 10 \times 0.3$ cm^3) and related burn-through and ignition times were monitored by an InfraRed camera (NEC Avio Infrared Technologies CO., Ltd., Thermo Gear G100/G120, Tokyo, Japan) and a digital data acquisition system. The configuration of the experimental setup is reported in Supplementary Figure S1.

The flammability of epoxy nanocomposite was assessed by UL-94 vertical burning tests (IEC 60695-11-10, sample of $13 \times 125 \times 3$ mm^3).

Mechanical characterization

The mechanical behaviour of the proposed material was investigated under tension and flexural loading conditions at room temperature (22 ± 1 °C) and 50 ± 3% relative humidity. All the specimens were realized by using a silicone die and cured at controlled humidity and temperature. First, several three-point bending tests were carried out in accordance with the ASTM D790[24]. An MTS Insight 30 electromechanical testing system was used undergoing position control at a crosshead displacement rate of 1.4 mm/min. The bar shaped specimens

have a nominal width b of 12.5 mm, thickness h of 3 mm, and length l equal to 70 mm. A support span length L_s of 50 mm was adopted.

The bending modulus of elasticity is calculated from the following relationship based on the classical beam theory approach[24]:

$$E_f = \frac{mL_s^3}{4bh^3} \tag{1}$$

where m is the slope of the tangent to the initial straight-line part of the load-deflection curve.

Secondly, experimental tensile tests were performed according to ASTM D638 standard[25] on dog-bone specimens with nominal thickness of 3 mm, width equal to 13 mm, and total length of 170 mm (Supplementary Fig. S2). The crosshead speed was set to 4 mm/min. The nominal tensile stress σ_t is obtained as the traction load per unit area of minimum original cross section, whilst the tensile strain ε_t is acquired from strain gauge. The Young's modulus E is calculated as the ratio of nominal stress to corresponding strain below the material proportional limit, whilst the Poisson's ratio v is evaluated using measurements results of strain gauge tee rosette. Sensors with grid length of 3 mm, nominal resistance of 350 , and maximum elongation of 5% were used. A data acquisition system HBM QuantumX 1615B was employed for recording the strain gauge measurements, the applied load and crosshead displacement signals during tensile tests. A trigger from HBM device was adopted to synchronize data signals with image acquisitions. The precision of strain gage acquisition was $\pm 10^{-6}$ mm/mm. No temperature changes affected strain gauge measurements.

Speckle pattern validation

The biochar particles and particle aggregates randomly dispersed in the volume of the specimens form a kind of speckle pattern. The quality of the pattern was evaluated by means of two parameters, i.e. the coverage factor (CF), or the ratio of black/grey pixels over the whole number of pixels, and the mean intensity gradient (MIG) value[26]. An optimal CF guarantees a suitable number of speckles to provide reliable data without confusion in the correlation process. The MIG parameter is related to the brightness variation across the speckle pattern. If the intensity is extremely uniform, the DIC software can lead to poor correlation findings. On the contrary, a high contrast between speckles and background can improve measurements accuracy. Both parameters were computed by using Matlab software. As the acquired images are monochrome and the base color of epoxy resin is not pure white, a threshold was chosen to count bright pixels. The mean intensity gradient parameter of an image of dimensions m x n pixels is expressed as:

$$\mathrm{MIG} = \frac{\sum_{i=1}^{m}\sum_{j=1}^{n}\sqrt{g_x\left(x_i,\ y_j\right)^2 + g_y\left(x_i,\ y_j\right)^2}}{m\ \cdot\ n} \tag{2}$$

where g_x and g_y are the grey-level intensity gradients of pixel (x_i, y_j) in the direction x and y, respectively.

The in-plane displacements and strains of tensile samples were acquired by means of the digital image correlation (DIC) technique. The *Ncorr*algorithm[27], implemented an in house made Matlab routine, was adopted to perform two-dimensional (2D) DIC analysis. A rectangular region of interest (ROI) was considered to assess horizontal u and vertical v displacements and to calculate longitudinal and transverse strains. The ROI is placed on the opposite side of specimen with respect to the strain gauge location, and its centre is coincident with the middle of sensor.

Images were acquired by a vision system composed of a monochrome IDS U-eye UI-1480SE- M-GL camera with 4.92 Mpixel of resolution, annular LED light, Pentax lens and micrometric motorized linear stages by MICOS. The adopted lights are suitable for a uniform illumination of samples without heating effect, while the positioners are useful to facilitate focusing and to place camera in front of the centre of strain gauge location. The image area was set up to acquire the portion of specimen that includes the strain sensor. The resulting scale conversion factor was 20 µm/pixel. A frame rate of 2 fps was adopted. The dimensions of the field of view were about 51 mm x 38 mm, whilst an 8 mm x 12 mm rectangular ROI was considered. Some rigid-body translation tests were carried out to evaluate the displacement accuracy of the testing set-up.

Finally, a comparison between strain response by strain gauges and the one by DIC analysis was performed to show the effectiveness of results obtained by using the speckle patterns of proposed material. Being a traditional contact technique for strain measurements based on strain gauge sensors, their acquisitions were selected as reference, although experimental uncertainty can affect them as well, and the mean square percentage error (MSPE)[28] was adopted to assess the quality of DIC outputs

$$MSPE = \frac{1}{p}\cdot\sum_{i=1}^{p}\left(\frac{y_i - \bar{y}_i}{y_i}\right)^2 \tag{3}$$

where y_i is the measure by strain gauge, $\bar{y}_i$ is the result by DIC technique at the same time instant and p is the number of acquired measurements.

Accelerated ageing of epoxy nanocomposite

The durability of nanocomposite was assessed by accelerated ageing tests using thermal ageing interior conditions according to ASTM D1183 standard[29]. Such conditions are usually adopted for studying the ageing of adhesively bonded joints and the matrix degradation of FRP composites[30]. A circulating air oven was used to apply

Test Condition Designation	Period [h]	Temperature [°C]
A	24	23
	24	46
	72	23
	48	46
B	48	57
	48	37
	8	−18
	64	37

Table 1. Interior test conditions.

Sample	1	2	3
	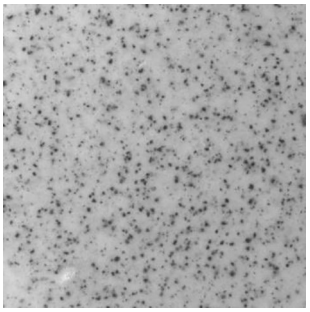	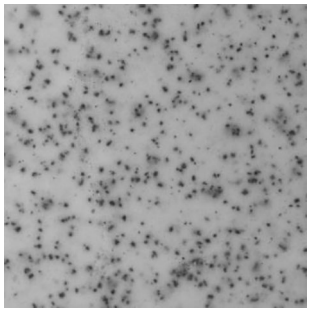	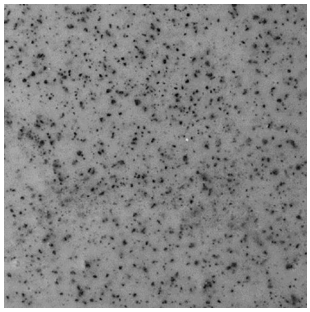
Biochar wt%	0.6	0.9	1.2
CF [%]	9	12	20
MIG	28	24	33

Table 2. Images of speckle patterns, content of biochar and TiO_2 (referred to the total mass of DGEBA and IDA) and DIC speckle pattern quality parameters (coverage factor, CF, and mean intensity gradient, MIG). The images size is 1200 × 1200 px.

sequences of controlled heating temperatures over required periods. A laboratory freezer was instead utilized to cool the specimens. Additional thermocouple and humidity probes were adopted to verify the stability of cyclic accelerated conditions. Temperature levels in heating were always lower than the glass transition temperature (Tg) of the ETiB epoxy nanocomposite. The adopted temperatures and the duration of the respective steps are shown in Table 1.

Results and discussion

Identification of the optimal composition for DIC patterns

With the aim of optimizing the workability of the mixture, in terms of pourability and ease of deposition, and overall quality of speckle pattern, in terms of black dots coverage, contrast, and randomly distributed speckles, several formulations were prepared with different mass ratios among the constituents (biochar and TiO_2). The TiO_2 content was first optimized, as its increase resulted in higher mean intensity gradient parameter and better greyscale contrast, and fixed at 2.9 wt%. Then the effect of biochar content was evaluated. The pattern quality parameters of the corresponding samples were analysed and reported in Table 2.

The random distribution of speckles in the matrix is one of the main requirements for a good DIC pattern[2]. This requisite appears satisfied in all prepared nanocomposites, as shown by the images displayed in Table 2. Aggregations of particles may occur during the preparation procedure, making the speckles size not entirely uniform. It was observed that an increase in the amount of coffee biochar led to a better coverage factor, so its content was raised up to 1.7 wt%. It is worth noting that the granulometry of coffee biochar can be varied during manufacturing process. Therefore, it can be scaled based on the type of application to obtain the most suitable speckle sizes for the requested measurement precision. Finally, being hypothesized a use in the composite repair of systems that can operate in a wide range of temperatures, the composition of the proposed resin was engineered also to enhance its fire retardant properties.

Physicochemical and thermal characterization of coffee-derived biochar and epoxy nanocomposites

The chemical composition of the biochar and related epoxy-based nanocomposite was studied by FTIR spectroscopy. The FTIR spectrum of coffee biochar is shown in Supplementary Figure S3. It contains a variety of vibrational bands, including those related to O-H stretching around 3380 cm^{-1}, with a possible contribution of N-H groups at lower wavenumbers, C-H stretching bands between 2950 and 2850 cm^{-1}, a wide band centred at 1580 cm^{-1}, mainly attributed to C = C stretching, with a shoulder at 1700 cm^{-1} that suggests the presence of

carbonyl or carboxyl groups, and some overlapping and poorly resolved bands between 1400 and 1100 cm^{-1}, ascribable to the carbon-based network and C-O bonds. These features hint at a prevalently aliphatic structure and abundant functional groups of the biochar sample. The FTIR spectrum of the TiO_2 particles (Supplementary Fig. S3) shows the typical broad band due to Ti-O-Ti stretching below 900 cm^{-1} and the bands related to O-H stretching and H-O-H bending, suggesting the presence of surface Ti-OH groups beside adsorbed water.

To confirm the completeness of the curing process of ETiB and examine its viscoelastic behaviour, DSC measurements were performed (Fig. 2a). The absence of any residual exothermic peak during the first heating ramp proves that the epoxy system is well cured. The Tg of ETiB is around 95 °C, which is higher compared to the value of about 85 °C found for the pristine resin (see Fig. 2a)[31]. This beneficial effect on the Tg may be due to the establishment of hydrogen bonds between the hydroxyl groups present on the surface of titania particles and biochar (see Supplementary Figs. S3 and S4) with the ones generated from the curing of the epoxy rings. These interactions result in a slightly increased stiffness of the polymer matrix, owing to the reduced mobility of the packed chains in the network[32,33]. The FTIR spectrum recorded for ETiB does not show the typical stretching bands at 970, 913, and 870 cm^{-1} of free oxirane groups (Fig. 2b), fully disappearing in well cured epoxy composites[34]. On the other side, the curing process leads to the presence of O-H stretching vibrations at 3400 cm^{-1}, responsible for the secondary interactions between the polymer matrix and the fillers. The identification of the other vibrations confirms the consistency of the chemical composition of ETiB as an epoxy-based nanocomposite[32]. In the spectrum of ETiB, the characteristic features of the two fillers are not easily observable, because of their low amount and the overlap between the vibrational frequencies of coffee biochar and epoxy matrix[35].

The thermal behaviour of ETiB was investigated by TGA measurements under nitrogen and air atmosphere (Fig. 2c and d). Figure 2c; Table 3 reveal that the addition of $TiO_2$and biochar does not significantly affect the thermal profiles of the epoxy matrix, which decomposes through mechanisms similar to those reported for epoxy resins cured with aliphatic amines[36]. In nitrogen atmosphere, ETiB degrades through a main step at around 369 °C, which is higher than the typical value (350 °C) observed for epoxy aliphatic systems[37]. Also, the residual char formed after the pyrolytic process appears slightly higher compared to the one that is usually recorded for pristine resin (~ 6 wt%)[38]. The weak acidic characteristics of TiO_2influence the pyrolytic decomposition of ETiB, promoting the dehydration of the polymer matrix and its charring behaviour[39]. However, the char produced during the decomposition in air atmosphere of ETiB does not appear thermo-oxidatively stable (Table 3),

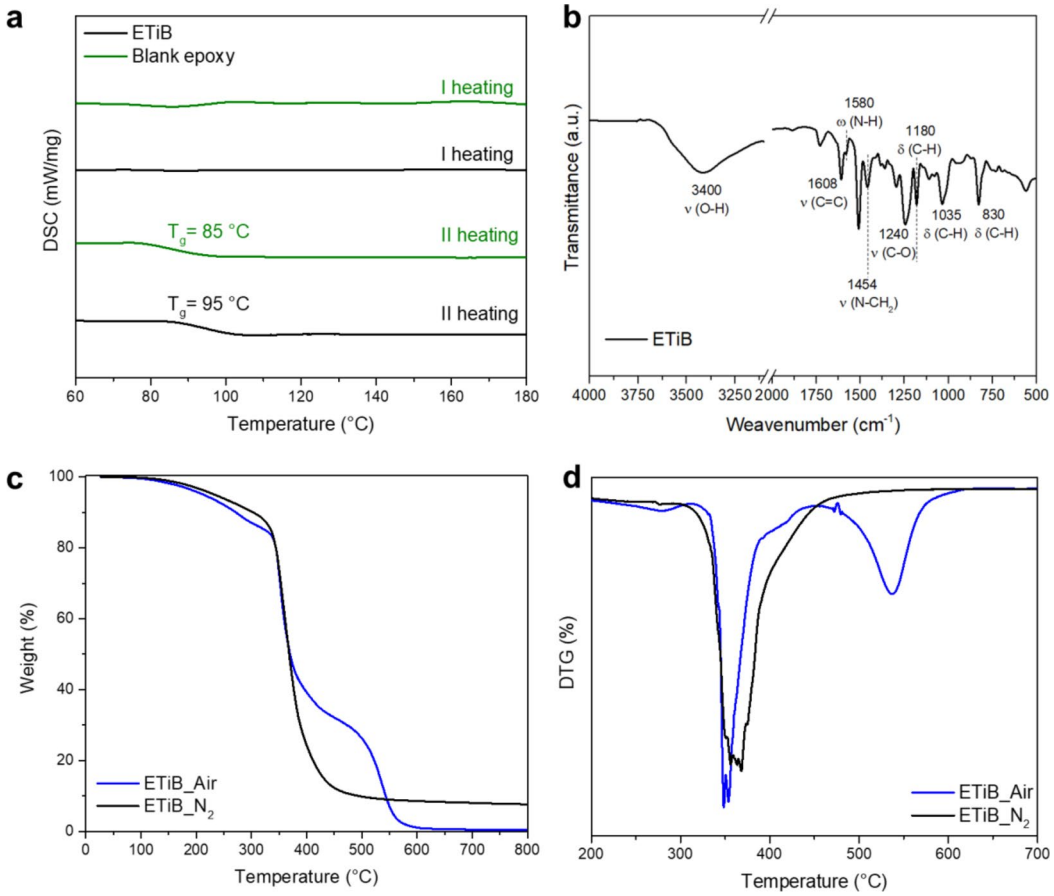

Fig. 2. DSC curves recorded in nitrogen on the ETiB nanocomposite (**a**), FTIR spectra of ETiB (**b**), TGA (**c**) and DTG (**d**) curves of ETiB recorded under nitrogen and air condition.

Sample	$T_{5\%}$ (°C)	T_{max1} (°C)	T_{max2} (°C)	Residue (wt%) at		
				T_{max1} (°C)	T_{max2} (°C)	800 °C
Nitrogen						
ETiB	210	369	-	51	-	8
Air						
ETiB	213	348	537	75	13	0

Table 3. TGA analysis of all samples in air and in N_2. $T_{5\%}$ is the temperature at which 5 wt% loss was recorded. T_{max} is the temperature at which the weight loss rate reached the maximum; the residues at T_{max} and 800 °C are also reported.

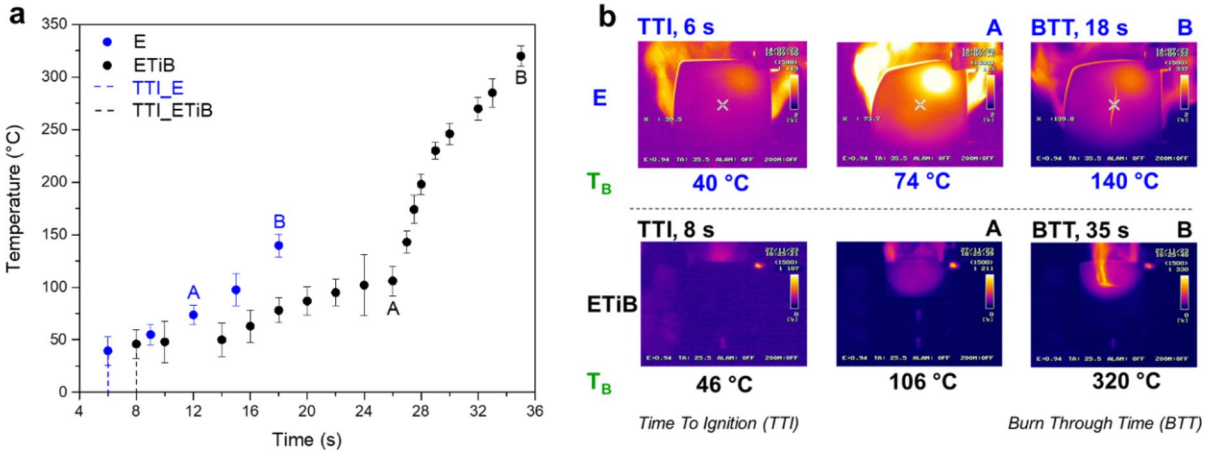

Fig. 3. Back temperature (T_B) profile along the time collected for ETiB (**a**). IR-images of samples captured at different instants during burn-through test (**b**). The dotted lines indicate the values of T_B at which the samples capture the flame, and the flaming combustion takes place. The corresponding time is called time to ignition (TTI). Burn-through time (BTT) represents the time at which the material loses its structural integrity.

revealing that this carbonaceous product acts more efficiently as barrier toward the thermal radiation, rather than the oxygen diffusion.

Fire behaviour of the epoxy nanocomposite

Epoxy resins are highly flammable therefore, to fulfil specific safety requirements (e.g., structural integrity at high temperatures or during flame exposure), flame retardant additives are widely employed[39]. In this context, the use of biochar associated with metal oxides was shown to improve the fire behaviour of epoxy composites[21]. Therefore, the fire behaviour at the surface of ETiB was assessed by means of the burn-through test, according to methodology and configuration reported in Supplementary Figure S1[40]. The fire response of ETiB was compared with the one of an unfilled resin (E). In a typical test, the flame tip of a gas blowpipe was applied to the middle of the sample surface till the appearance of visible cracks or holes throughout the epoxy matrix[41]. Along the flame application, the back temperature (T_B) profile at the sample surface was recorded by employing an IR camera. Also, the time required to observe the loss of structural integrity of samples was detected and identified as burn-through-time (BTT). Figure 3 reports the $T_B$along the time and BTT for E and ETiB, together with the IR-images of the samples at different times. The flame application to the surface of the material triggers its decomposition, which leads to the start of a flaming combustion when the oxygen concentration in the gas phase becomes higher than the lower flammability limit[42]. The flaming combustion of E and ETiB and the formation of holes are strongly related to the heat transfer phenomena taking place at their surface. Figure 3a reveals that the addition of TiO_2 particles and biochar into the polymer matrix results in a significant increase (~ 33%) of the time to ignition (TTI), which is the time required for the start of the flaming combustion. Besides, E captured the flame at T_B= 40 °C, while ETiB at a value of around 46 °C and only after a longer TTI. Unlike E, ETiB lost its structural integrity at a T_B of about 320 °C, also achieving a T_B= 140 °C very slowly and after almost a double timespan (~ 28 s) compared to the pristine system (Fig. 3a and b). Finally, Fig. 3b displays that the BTT of ETiB is ~ 94% higher than the one of E, which additionally supports the fire retardant action of fillers, delaying the thermal degradation of the material and its flaming combustion at the surface. These results may be ascribed to synergistic flame retardant mechanisms exerted by the fillers in the condensed phase during the first stages of the decomposition process. In particular, during the combustion of ETiB, TiO_2particles boost the formation of an abundant and refractive pyrolytic char, in agreement with TGA results collected under nitrogen atmosphere, containing titania substructures and acting as thermal insulator, while the presence of char residues lowers the heat transfer at the surface and thus the oxidative degradation with flame generation of the epoxy matrix[43,44]. The

presence of hydroxyl groups and oxygen functional groups on the surface of titania particles and coffee biochar promote the dehydration of the epoxy matrix and the production of char during the combustion process. As also reported in the literature[21,45], this char, formed in presence of titania particles, contains titanium-based species. The ceramic and refractive character of this char, together with its high graphitization degree, confer superior thermal insulation properties and fire shielding capability to the carbonaceous residue.

As shown in Fig. 4a, the biochar used for the preparation of ETiB is characterized by the Raman spectrum profile of a highly disorganized carbon with an I_D/I_G ratio of up to 2.5 while the ETiB residue obtained after burn-through test (Fig. 4b) is more organized with an I_D/I_G ratio of up to 1.3. As reported by Tunistra et al.[46], I_D/I_G ratio can be used to evaluate the average volume of graphitic crystallites (L_a) showing that L_a is 18 and 34 Å for BC and ETiB, respectively, that are still far from the size typical of a highly graphitic carbon[47]. Nevertheless, the more graphitic carbon formed act as physical barrier for both thermal flux and oxygen diffusion[48,49]. Accordingly, the simultaneous presence of both disorganized graphitic carbon together with the presence of TiO_2promote the thermal phonon confinement reducing the heat diffusion in the materials[50–52].

The residual char of ETiB produced after the burn-through test was also analysed by FTIR (Fig. 4c). The structure of the epoxy matrix appears largely preserved in the char, however the presence of aromatic structures is confirmed by the peaks at 638 cm^{-1}, 802 cm^{-1}, and 871 cm^{-1}, related to aromatic C–H out-of-plane vibrations in meta, para, and ortho, respectively[53,54]. The finding of such species and the C=C stretching vibration at 1577 cm^{-1} support a notable carbonization via dehydration of epoxy resin, also promoted by the acidity of TiO_2[38,55]. Finally, the stretching vibration broad band around 600 cm^{-1}, linked to Ti-O-Ti linkages of titanium-based polymeric substructures, gives further evidence of the formation of a ceramic char rich in titania particles[44,56,57] as also proved by the signal centred at 628 cm^{-1} in the Raman spectrum (Fig. 4b)[58].

In view of the above, the use of titania particles and coffee biochar is not only suitable for the manufacturing of epoxy coatings providing proper and functional patterns but also confers improved thermal insulating and flame retardancy features to the polymer matrix and final product. The flammability of ETiB was studied through the application of the UL-94 vertical burning test. The vertical flame spread was evaluated on five specimens,

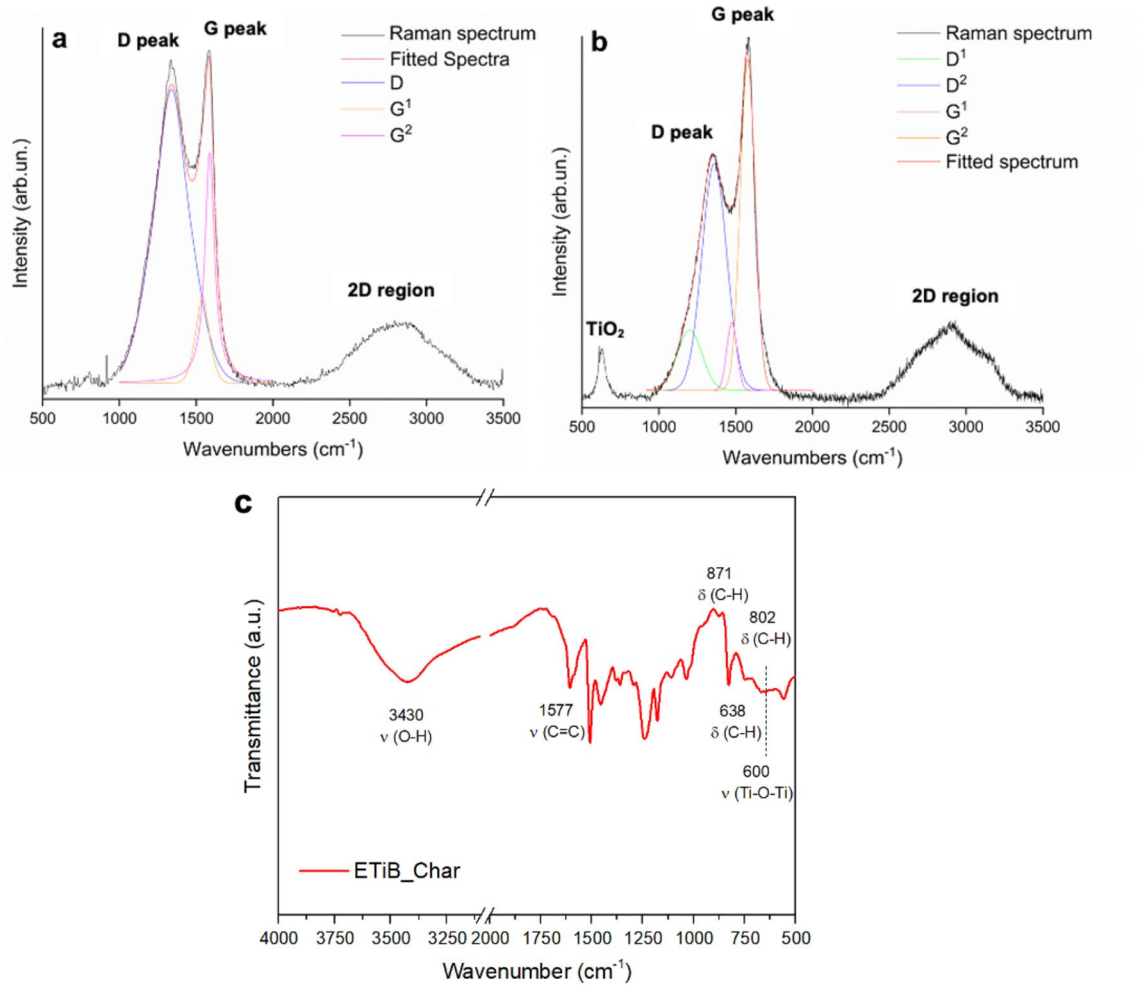

Fig. 4. Raman spectra of biochar (**a**) and ETiB char residue after burn-through test (**b**) in the range between 500–3500 cm^{-1}. Spectra were fitted in the range 1000–2000 cm^{-1} as reported by Tagliaferro et al.[23]. FTIR spectrum of char residue (**c**).

Element	Biochar (wt%)	ETiB (wt%)	ETiB residue (wt%)
C	72	78	54
O	28	21	22
Ti	0	1	24

Table 4. EDX elemental analysis of biochar, ETiB and ETiB char residue after burn-through test.

Sample	Young's Modulus [GPa]	95% C.I. [GPa]	Poisson's ratio	95% C.I.	Tensile stress [MPa]	95% C.I. [MPa]	Bending modulus of Elasticity [GPa]	95% C.I. [GPa]	Bending stress [MPa]	95% C.I. [MPa]
Pristine resin	1.92 ± 0.05	0.07	0.36 ± 0.01	0.01	34 ± 11	14	2.66 ± 0.27	0.26	89 ± 7	7
ETiB	2.95 ± 0.19	0.15	0.36 ± 0.01	0.01	21 ± 3	2	3.13 ± 0.37	0.36	42 ± 9	8
Aged ETiB (A)	2.15 ± 0.05	0.05	0.38 ± 0.02	0.03	23 ± 3	4	-	-	-	-
Aged ETiB (B)	2.54 ± 0.43	0.48	0.37 ± 0.01	0.02	21 ± 5	5	-	-	-	-

Table 5. Mechanical properties in bending and tension of as prepared and aged samples.

according to the standard requirements. All the investigated samples cannot be classified, as they do not give self-extinction before the flame reaches the holding clamp. However, unlike in the case of the neat epoxy resin, the presence of titania particles and coffee biochar in ETiB prevents the occurrence of melt dripping phenomena during the flammability test. The absence of dripping and melt flowing of the pyrolyzing polymer is highly desired in several applications, as this feature avoids the starting of a pool fire and additional ignitions. These findings well agree with similar results observed in other research works reported in the literature[59]. It is well known that the addition of micro- or nano-particles to plastics and thermosets can prevent the triggering of dripping phenomena, owing to the increase of the melt viscosity of the burning system, hindering the generation of incandescent drops[59]. The above considerations additionally support the formation of a continuous and abundant char during the combustion of the epoxy nanocomposite material, mainly due to the presence of the functional fillers (TiO_2 nanoparticles and coffee BC) as indicated by EDX data in Table 4. More in detail, BC shows a very high oxygen content due to the presence of residual oxygen rich functionalities, while the ETiB residue displays a notable decrement of carbon content and an increase of the titanium one, linked to titania species. This well agrees with the formation of a char protective layer as consequence of polymeric matrix consumption. As evidenced by SEM images, ETiB does not show any trace of original biochar particles (Supplementary Fig. S4a) but small carbon flakes due to the disaggregation of the biochar itself[60] as shown by the magnifications of ETiB surface (Supplementary Fig. S4b) and confirmed by the average diameter of BC particles, peaked at 34.6 µm (Supplementary Fig. S5). The char residue of ETiB exhibits a morphology that suggests the production of carbon black like materials from the polymeric matrix homogenously mixed with biochar and TiO_2 (Supplementary Fig. S4c and Table 4). After the assessment of the physicochemical and fire properties of the selected nanocomposite, its mechanical and functional performances were evaluated.

Mechanical tests results

The results of mechanical experiments of ETiB nanocomposite, thermally aged ETiB and pristine resin are provided in Table 5. The standard deviation, S.D., and the 95% confidence interval of the average value, C.I., are evaluated using the procedures provided by the ISO 2602 standard[61]. No significant scatter in the mechanical properties was observed overall. The percentage difference in terms of tensile strength and bending stress between the base material and the one containing biochar and $TiO_2$was about 40% and 50%, respectively. On the other hand, ETiB resulted in a higher axial and bending stiffness with respect to the base resin. The enhancement of stiffness in epoxy composites can result from interactions between fillers and matrix, for example by improving interfacial bonding, as observed in presence of metal oxide fillers that show high surface area, thermal stability, and phase stability[62].

After the thermal ageing no significant change in colour of specimens' surface due to thermo-oxidation phenomenon was clearly visible. This could be ascribable to the temperature levels of the conditioning procedures, which were always lower than the Tg of the material[30]. The tensile tests on thermally aged ETiB specimens did not evidence any noticeable difference in tensile strength with respect to the untreated samples, while a moderate and slight difference in terms of Young's modulus was shown for conditioning types A and B, respectively. The differences between the measurements by optical and traditional methods highlighted a negligible significance of the alteration of the speckle pattern for its proper use with the DIC technique.

The resulting average values of elastic modulus fall within the common range of epoxy resins for civil and industrial structural reinforcement. The stress-strain curves are plotted in Fig. 5, highlighting that the material behaved as fragile. Moreover, some samples, both aged and untreated, showed a non-linear stress-strain behaviour.

It is worth noting that fracture surfaces of most specimens that reached smaller tensile strength exhibited an agglomeration of biochar particles, as shown in Fig. 6. If on the one hand, localized aggregate densification represents a drawback as possible damage onset of polymer matrix, on the other hand it can be assimilated to

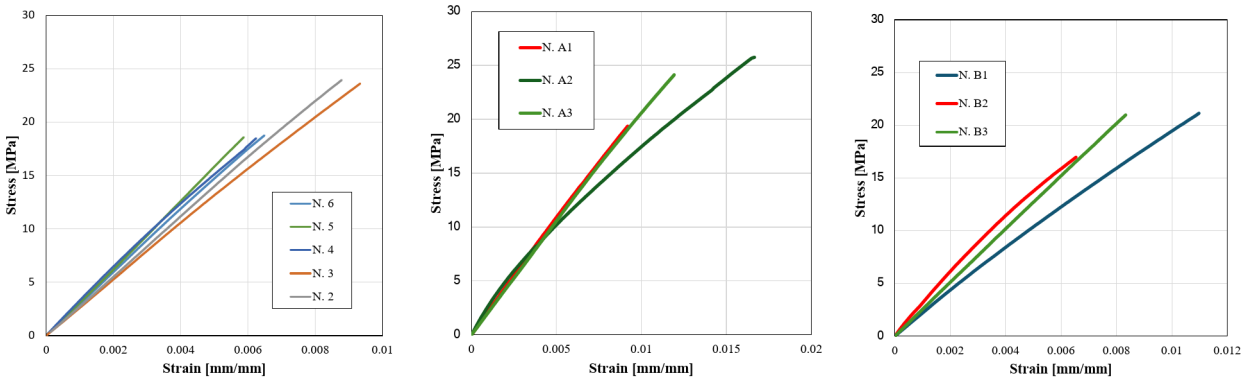

Fig. 5. Stress-strain curves from tensile tests. Strain values were taken from strain gauges output. (**a**) untreated specimens; (**b**) Type A thermally aged specimens; (**c**) Type B thermally aged specimens.

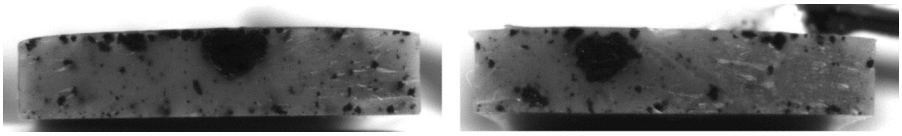

Fig. 6. Fracture surfaces of ETiB specimen N. 6 and thermally aged ETiB specimen N. A1.

air voids that can commonly occur in the manufacturing process of FRP composites, thus acceptable from a practical standpoint.

However, the aggregation of the biochar particles, due to interactions between the abundant polar groups on their surface (see Sect. Physicochemical and thermal characterization of coffee-derived biochar and epoxy nanocomposites), may be avoided by adopting suitable strategies along the manufacturing process. Advanced mixing techniques, involving sonication or high-energy stirring of the mixture before casting or coating could improve the dispersion of the particles in the polymer matrix. Alternatively, a proper functionalization of their surface could lead to a better chemical affinity between biochar and epoxy chains, for example by grafting less polar species, such as aliphatic groups, through the condensation of an alkyl silane.

DIC analysis outcomes

The speckle patterns obtained by means of the addition of biochar particles were analysed to assess their quality (Fig. 7). Speckles resulted randomly distributed and of dimensions greater than 3-by-3 pixels, which is the minimum size commonly accepted to prevent aliasing effect[63]. A coverage factor ranging from 29 to 40% was obtained. Some voids due to air inclusion are visible on the samples surface. The large value of mean intensity gradient parameter of the tested speckle patterns, calculated by Matlab and ranging from 27 to 48[26], further confirmed a positive evaluation of their global quality. Histogram and particle size distribution, in terms of equivalent circular area diameter, of a representative speckle pattern are reported in Supplementary Figure S6.

Rigid translations of specimen were applied to evaluate quality and accuracy of measurements. The results of DIC analysis with a translation of 2 mm showed that the measured average value exhibited a difference of 0.012% from the assigned displacement, whilst a maximum difference in displacement measurements lower than 0.25% was highlighted with a subset radius of 60 px, a subset spacing of 3 px, and six threads. A complete sensitivity analysis was previously performed on rigid translation assessment to select camera calibration parameters, lighting conditions, field of view dimension, and correlation algorithm settings (see Supplementary Table S1).

In addition, DIC analyses were performed to carry out the strain response of ETiB material. Contour plots of measurements by DIC, as reported in Fig. 8, showed quite uniform bands representative of effective polymer behaviour in traction, i.e. elongation in loading direction and transverse contraction.

The strain values obtained from DIC analysis were compared with acquisitions from strain gauges showing a satisfactory agreement. In Fig. 9a the comparisons of L and H strain response trends are presented for a representative tensile test (specimen N.4). Data by DIC were not filtered or interpolated to obtain the tensile behaviour plotted in Fig. 9b. The scatter of stress-strain data resulted quite small. The linear interpolation of linear region points of the stress-strain data sets in Fig. 9b carried out a slope corresponding to Young's modulus by DIC strain outputs, from which an average value of 2.80 ± 0.27 GPa (C.I. equal to 0.27 GPa) was carried out for the batch of four specimens considered, i.e. samples N. 2, N.3, N. 4, and N. 5.

Furthermore, the average value of Poisson's ratio from DIC analysis outcomes resulted equal to 0.38, with a standard deviation and a C.I. of ± 0.01 MPa. These results are in sound agreement with the ones by using

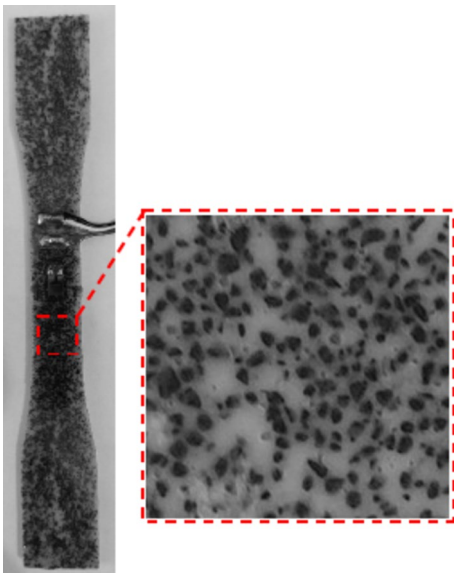

Fig. 7. Representative speckle pattern provided by ETiB material. Close up view: image size 300 × 300 px, CF = 38%, MIG = 48.

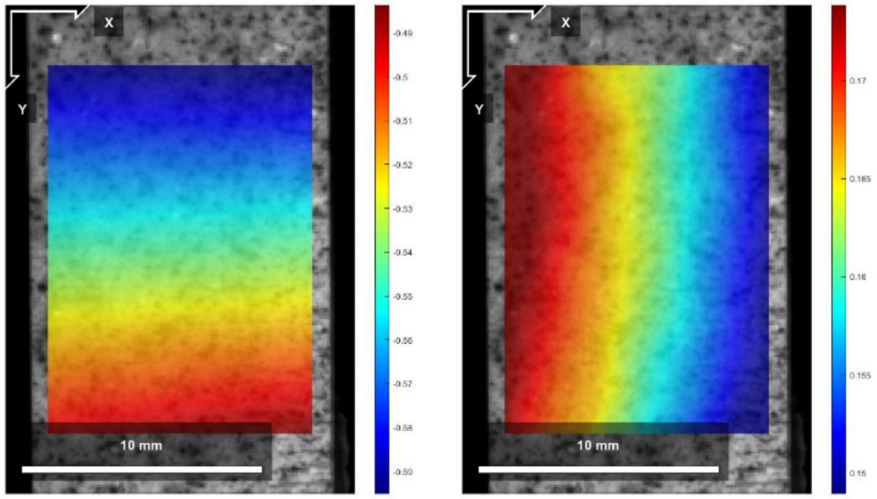

Fig. 8. DIC displacement outputs at an intermediate stage of tensile test. The bar scale is 10 mm.

strain gauges acquisitions. Despite of a larger scatter of the results of tests on aged specimens with respect to the untreated ones, a satisfactory comparison of acquisition by strain gauges and outcomes from DIC analyses can be observed in Figs. 10 and 11.

The modulus of elasticity obtained from data set by DIC analysis of aged specimens resulted 2.60 ± 0.13 GPa (C.I. equal to 0.15 GPa) and 2.51 ± 0.28 GPa (C.I. equal to 0.32 GPa) for A (specimens N. A1, N. A2, and N. A3) and B (specimens N. B1, N. B2, and N. B3) conditioning procedure, respectively. Therefore, a good agreement with results of Table 5 is provided.

Table 6 shows the differences of deformation trend response, both longitudinal *L* and horizontal *H* strains, by two methodologies in terms of MSPE. More specifically, a tee rosette was bonded on specimen N.2, N.3 and N.4, whilst a uniaxial strain gauges in the loading direction *L* was installed on the other samples. All the thermally aged samples were equipped with a tee rosette. The value of MSPE parameter, lower than 5%, corroborates the effectiveness of the presented speckled material for monitoring purposes.

Conclusions

Following a green manufacturing approach, a novel epoxy-based nanocomposite material (ETiB) was designed and prepared using TiO_2 nanoparticles and biochar from waste spent coffee grounds as fillers. The incorporation of the additives in the epoxy resin raised the Young's modulus by around 30% with respect to pristine resin,

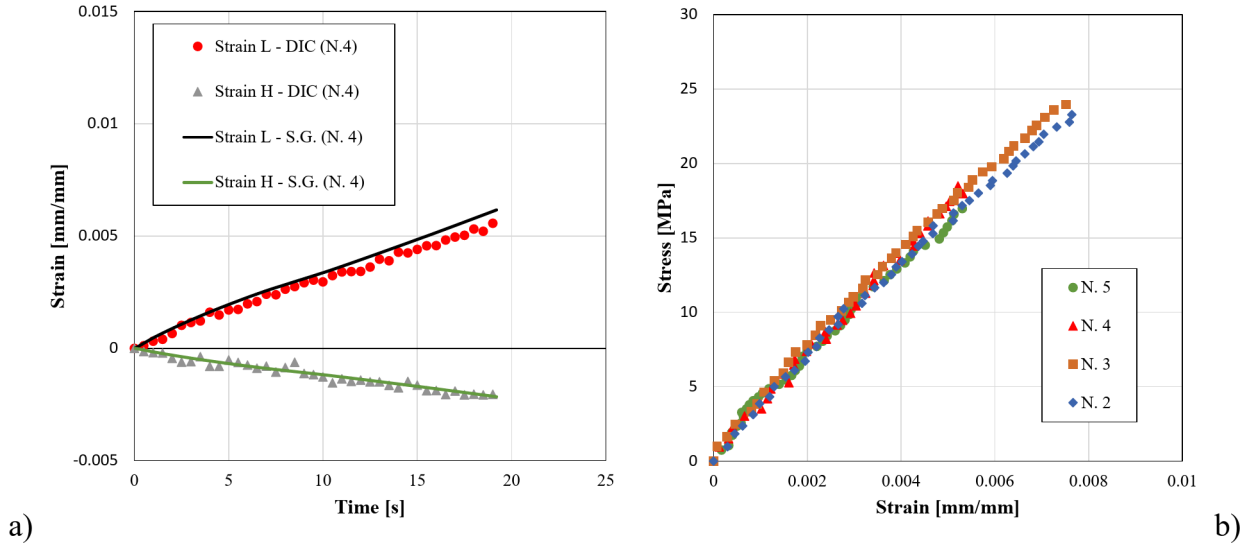

Fig. 9. (**a**) Representative comparison of *L* and *H* strain trends from a tensile test (specimen N.4), (**b**) Stress-strain curves obtained from DIC outcomes.

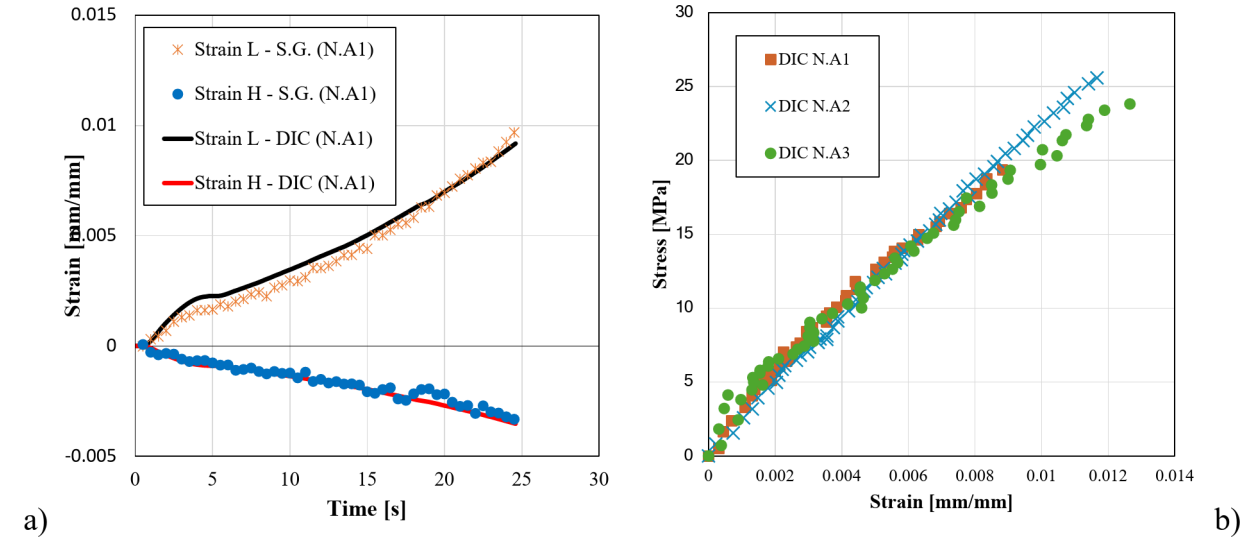

Fig. 10. (**a**) Representative comparison of *L* and *H* strain trends from a tensile test of type A ageing condition (specimen N. A1), (**b**) Stress-strain curves obtained from DIC outcomes of specimens subjected to type A thermal ageing procedure.

whilst reduced the tensile strength by about 38%. The flammability at the surface of ETiB was also assessed, being the proposed nanocomposite designed for engineering applications with a wide operating temperature range. SEM-EDX analysis of the residual char highlights that biochar and TiO_2 particles exert a notable flame retardant action in the condensed phase.

The proposed engineered ETiB epoxy nanocomposite resulted suitable for the realization of efficient image speckle patterns to be used for DIC analysis. A comparison of DIC results with traditional strain gauges acquisitions was performed showing a good agreement. The resulting mean square percentage error (MSPE) was always less than 5%. The accuracy of the measurements by DIC technique can be considered as satisfactory for the assessment of most bonded composite repair applications in different engineering sectors. Although the randomness of biochar particles into the matrix could create zones of the speckle pattern with lower cover factor, the ease of use as a FRP composite matrix could make this material promising for monitoring the durability of structural bonded repairs, keeping good performances and sustainability features. Within this context, the degradation of ETiB was investigated under thermal aging conditions. Heating cycles, below the material transition glass temperature and up to 60% of Tg, and cycles of freezing as well were applied to verify the effectiveness of speckle patterns subjected to accelerated aging process. The findings on the aged patterns provided a preliminary proof of concept of the usefulness of the new epoxy-based nanocomposite for DIC

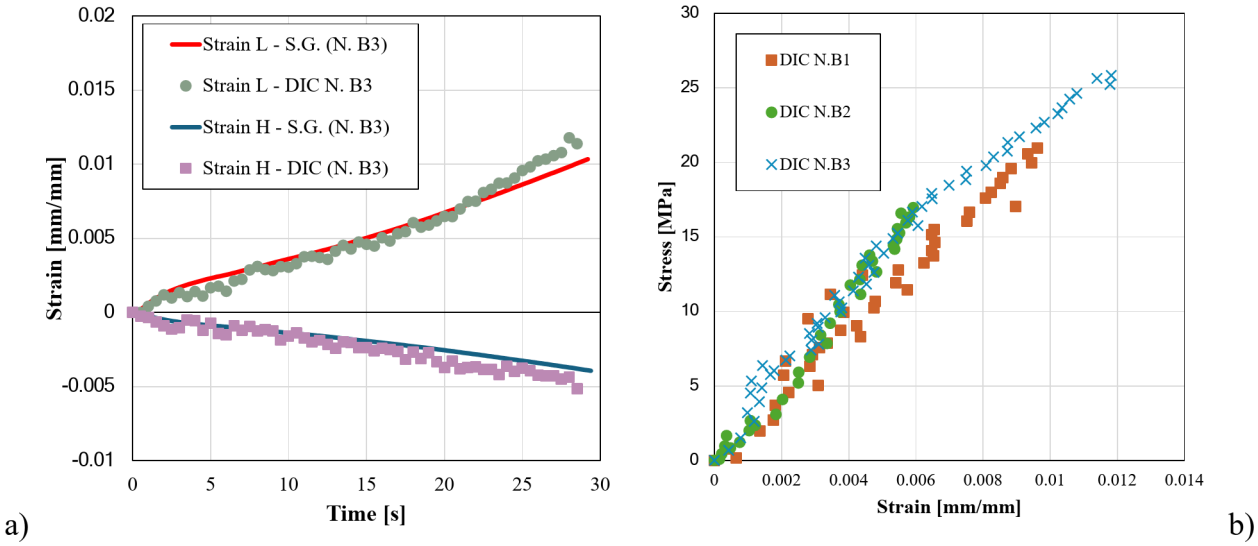

Fig. 11. (**a**) Representative comparison of *L* and *H* strain trends from a tensile test of type B ageing condition (specimen N. B3), (**b**) Stress-strain curves obtained from DIC outcomes of specimens subjected to type B thermal ageing procedure.

Specimen #	MSPE Trend of L strain [%]	MSPE Trend of H strain [%]
2	1.3	2.9
3	3.4	2.0
4	1.5	2.8
5	0.4	-
6	0.5	-
A1	2.9	0.4
A2	2.4	4.5
A3	4.7	3.8
B1	0.3	1.9
B2	4.6	4.3
B3	4.3	0.9

Table 6. Mean square percentage error (MSPE) from comparison of DIC outputs with strain gauges acquisitions.

analysis. Considering its available, inexpensive and partially bio-based components as well as the easily scalable pyrolysis treatment for biochar production, a good potential for the large-scale application of this material is envisaged. This study may pave the way to the design of new products for the monitoring of deformations, fulfilling a circular economy requirement, by the reuse of waste materials in high technological applications. Finally, the proposed material may be used in structural health monitoring applications for a continuous assessment of FRP strengthened structures to detect damage, crack, or fatigue occurrence over time, enabling proactive maintenance and enhancing safety of structures.

Data availability

The data that support the findings of this study are available from the corresponding author upon reasonable request.

Received: 12 November 2024; Accepted: 10 February 2025
Published online: 26 February 2025

References

1. Orteu, J. J. & Schreier, H. W. Digital image correlation (DIC), in: Image Correlation for Shape, Motion and Deformation Measurements, (2009).
2. Schreier, H., Orteu, J. J. & Sutton, M. A. *Image Correlation for Shape, Motion and Deformation Measurements: Basic Concepts, Theory and Applications* (Springer, 2009).

3. Mallya, R., Uchil, A. K., Shenoy, S. B. & Pai, A. Application of digital image correlation in aerospace engineering: structural health monitoring of aircraft components. *Aerosp. Syst.* 1–13. (2024).
4. Mousa, M. A. et al. Application of digital image correlation in structural health monitoring of bridge infrastructures: a review. *Infrastruct. (Basel).* **6**, 176 (2021).
5. Niezrecki, C., Baqersad, J. & Sabato, A. Digital image correlation techniques for non-destructive evaluation and structural health monitoring. *Handb. Adv. Non-Destructive Evaluation* **46** (2018).
6. Tehrani, A. D., Kohankar Kouchesfehani, Z. & Najafi, M. Pipe profiling using digital image correlation, in: Pipelines 2020, American Society of Civil Engineers Reston, VA, : 36–45. (2020).
7. Crammond, G., Boyd, S. W. & Dulieu-Barton, J. M. Dynamic analysis of composite marine structures using full-field measurement techniques. *J. Mar. Eng. Technol.* **13**, 23–35 (2014).
8. Caminero, M. A., Lopez-Pedrosa, M., Pinna, C. & Soutis, C. Damage monitoring and analysis of composite laminates with an open hole and adhesively bonded repairs using digital image correlation. *Compos. B Eng.* **53**, 76–91 (2013).
9. Caminero, M. A. et al. Using digital image correlation techniques for damage detection on adhesively bonded composite repairs. *Adv. Compos. Lett.* **21**, 096369351202100203 (2012).
10. Dong, Y. L. & Pan, B. A review of speckle pattern fabrication and assessment for digital image correlation. *Exp. Mech.* **57**, 1161–1181 (2017).
11. Palanca, M., Tozzi, G. & Cristofolini, L. The use of digital image correlation in the biomechanical area: a review. *Int. Biomech.* **3**, 1–21 (2016).
12. Kursun, E. C., Supreeti, S., Janssens, K. G. F., Schift, H. & Spätig, P. High optical contrast nanoimprinted speckle patterns for digital image correlation analysis. *Micro Nano Eng.* **17**, 100164 (2022).
13. Luong, P., Bonnaire, R., Périé, J., Sirvin, Q. & Penazzi, L. Speckle pattern creation methods for two-dimensional digital image correlation strain measurements applied to mechanical tensile tests up to 700° C. *Strain* **57**, e12388 (2021).
14. Verschatse, O., Van Paepegem, W., De Clerck, K. & Daelemans, L. Development of a versatile speckle pattern of nano-sized polymer particles for high-resolution SEM-DIC. *Polym. Test.* **125**, 108134 (2023).
15. Quino, G. et al. Speckle patterns for DIC in challenging scenarios: rapid application and impact endurance. *Meas. Sci. Technol.* **32**, 15203 (2020).
16. Xu, C. et al. Effect of wheat bran filler particulates nettle fiber reinforced epoxy matrix composite – A novel material for thermal insulation application. *Therm. Sci. Eng. Progress*. **55**, 102917 (2024).
17. Shahapurkar, K. et al. Flexural behavior of epoxy composites reinforced with banana fibers in different architectures: experimental, analytical, and numerical approaches. *Biomass Convers. Biorefin.* **14**, 21603–21618 (2024).
18. Ma, J. et al. Effect of inorganic nanoparticles on mechanical property, fracture toughness and toughening mechanism of two epoxy systems. *Polym. (Guildf).* **49**, 3510–3523 (2008).
19. Saludung, A., Ogawa, Y. & Kawai, K. Microstructure and mechanical properties of epoxy resin-reinforced geopolymer exposed to high temperatures. *Mater. Lett.* **331**, 133473 (2023).
20. Mensah, R. A. et al. A review of sustainable and environment-friendly flame retardants used in plastics. *Polym. Test.* **108**, 107511 (2022).
21. Bifulco, A. et al. Coffee waste-derived biochar as a flame retardant for epoxy nanocomposites. *Sustainable Mater. Technol.* **41**, e01079 (2024).
22. Forcina, A., Petrillo, A., Travaglioni, M., di Chiara, S. & De Felice, F. A comparative life cycle assessment of different spent coffee ground reuse strategies and a sensitivity analysis for verifying the environmental convenience based on the location of sites. *J. Clean. Prod.* **385**, 135727 (2023).
23. Tagliaferro, A., Rovere, M., Padovano, E., Bartoli, M. & Giorcelli, M. Introducing the novel mixed gaussian-lorentzian lineshape in the analysis of the raman signal of biochar. *Nanomaterials* **10**, 1748 (2020).
24. ASTM D790-17. Standard Test Methods for Flexural Properties of Unreinforced and Reinforced Plastics and Electrical Insulating Materials. ASTM International, USA.
25. ASTM D638-22. Standard test method for tensile properties of plastics. ASTM International, USA.
26. Pan, B., Lu, Z. & Xie, H. Mean intensity gradient: an effective global parameter for quality assessment of the speckle patterns used in digital image correlation. *Opt. Lasers Eng.* **48**, 469–477 (2010).
27. Blaber, J., Adair, B. & Antoniou, A. Ncorr: open-source 2D digital image correlation matlab software. *Exp. Mech.* **55**, 1105–1122 (2015).
28. Ciampolillo, S. & Loreti, M. Teoria degli errori e analisi dei dati: introduzione alle esperimentazioni di fisica I, Libreria Progetto, (1994).
29. ASTM D1183-03R19. Standard Practices for Resistance of Adhesives to Cyclic Laboratory Aging Conditions. ASTM International, USA.
30. Zhang, M., Sun, B. & Gu, B. Accelerated thermal ageing of epoxy resin and 3-D carbon fiber/epoxy braided composites. *Compos. Part. Appl. Sci. Manuf.* **85**, 163–171 (2016).
31. Venezia, V. et al. Detailed thermal, fire, and mechanical study of silicon-modified epoxy resin containing humic acid and other additives. *ACS Appl. Polym. Mater.* **3**, 5969–5981 (2021).
32. Choi, Y. M., Hwangbo, S. A., Lee, T. G. & Ham, Y. B. Effect of particle size on the mechanical properties of TiO2–epoxy nanocomposites. *Materials* **14**, 2866 (2021).
33. Goyat, M. S., Rana, S., Halder, S. & Ghosh, P. K. Facile fabrication of epoxy-TiO2 nanocomposites: a critical analysis of TiO2 impact on mechanical properties and toughening mechanisms. *Ultrason. Sonochem*. **40**, 861–873 (2018).
34. Kim, D. K., Choi, Y. H., Kim, K. W. & Kim, B. J. Transparent glass-fiber-reinforced epoxy composites and their optical characteristics. *Compos. Sci. Technol.* **232**, 109848 (2023).
35. El-Kattan, I. M., Saif, M. S., El-Hariri, M. O. R., Elgandy, A. H. & Pérez-Villarejo, L. Eliche-Quesada, assessing the individual impact of magnesia and titania nano-particles on the performance of alkali-activated slag mortars. *Constr. Build. Mater.* **365**, 130103 (2023).
36. Bifulco, A. et al. Improving flame retardancy of in-situ silica-epoxy nanocomposites cured with aliphatic hardener: combined effect of DOPO-based flame-retardant and melamine. *Composites Part C.* **2**, 100022 (2020).
37. Aouf, C. et al. Multi-functionalization of gallic acid. Synthesis of a novel bio-based epoxy resin. *Eur. Polym. J.* **49**, 1185–1195 (2013).
38. Bifulco, A. et al. In situ P-modified hybrid silica–epoxy nanocomposites via a green hydrolytic sol–gel route for flame-retardant applications. *ACS Appl. Nano Mater.* **6**, 7422–7435 (2023).
39. Bifulco, A., Imparato, C., Aronne, A. & Malucelli, G. Flame retarded polymer systems based on the sol-gel approach: recent advances and future perspectives. *J. Solgel Sci. Technol.* 1–25. (2022).
40. Bifulco, A. et al. Multifunctional fire-resistant and flame-triggered shape memory epoxy nanocomposites containing carbon dots. *Chem. Eng. J.* **484**, 149327. https://doi.org/10.1016/j.cej.2024.149327 (2024).
41. Ma, R., Shen, R., Quan, Y. & Wang, Q. Tunable flammability studies of graphene quantum dots-based polystyrene nanocomposites using microscale combustion calorimeter. *J. Therm. Anal. Calorim.* **147**, 10383–10390 (2022).
42. Tran, K. D. Burn-through resistance of fibre/felt materials for aircraft fuselage insulation blankets. *Fire Mater.* **26**, 1–6 (2002).
43. Ma, R., Shen, R., Quan, Y. & Wang, Q. Preparation of Graphene Quantum Dots Decorated Montmorillonite to Reinforce Fire Retardancy of Polystyrene. *Ind. Eng. Chem. Res.* **62**, 13510–13518 (2023).

44. Zhang, L., Huang, Y., Dong, H., Xu, R. & Jiang, S. Flame-retardant shape memory polyurethane/MXene paper and the application for early fire alarm sensor. *Compos. B Eng.* **223**, 109149 (2021).
45. Liu, C. et al. Modification of epoxy resin through the self-assembly of a surfactant-like multi-element flame retardant. *J. Mater. Chem. Mater.* **4**, 3462–3470 (2016).
46. Tuinstra, F. & Koenig, J. L. Raman spectrum of graphite. *J. Chem. Phys.* **53**, 1126–1130 (1970).
47. Morant, R. A. The crystallite size of pyrolytic graphite. *J. Phys. D Appl. Phys.* **3**, 1367 (1970).
48. Wang, X., Kalali, E. N., Wan, J. T. & Wang, D. Y. Carbon-family materials for flame retardant polymeric materials. *Prog Polym. Sci.* **69**, 22–46 (2017).
49. Araby, S. et al. Recent advances in carbon-based nanomaterials for flame retardant polymers and composites. *Compos. B Eng.* **212**, 108675 (2021).
50. Zhang, Z. et al. Size-dependent phononic thermal transport in low-dimensional nanomaterials. *Phys. Rep.* **860**, 1–26 (2020).
51. Zhu, K. R., Zhang, M. S., Chen, Q. & Yin, Z. Size and phonon-confinement effects on low-frequency Raman mode of anatase TiO2 nanocrystal. *Phys. Lett. A.* **340**, 220–227 (2005).
52. Arora, A. K., Rajalakshmi, M. & Ravindran, T. R. Phonon confinement in nanostructured materials. *Encyclopedia Nanosci. Nanatechnol.* **8**, 499–512 (2004).
53. Sun, Z., Hou, Y., Hu, Y. & Hu, W. Effect of additive phosphorus-nitrogen containing flame retardant on char formation and flame retardancy of epoxy resin. *Mater. Chem. Phys.* **214**, 154–164 (2018).
54. Bifulco, A. et al. Fire and mechanical properties of DGEBA-based epoxy resin cured with a cycloaliphatic hardener: combined action of silica, melamine and DOPO-derivative. *Mater. Des.* **193**, 108862 (2020).
55. Vahabi, H., Laoutid, F., Mehrpouya, M., Saeb, M. R. & Dubois, P. Flame retardant polymer materials: an update and the future for 3D printing developments. *Mater. Sci. Engineering: R: Rep.* **144**, 100604 (2021).
56. Kausar, A. Epoxy and quantum dots-based nanocomposites: achievements and applications. *Mater. Res. Innovations* (2019).
57. Wu, H. et al. An intramolecular hybrid of metal polyhedral oligomeric silsesquioxanes with special titanium-embedded cage structure and flame retardant functionality. *Chem. Eng. J.* **374**, 1304–1316 (2019).
58. Lottici, P. P., Bersani, D., Braghini, M. & Montenero, A. Raman scattering characterization of gel-derived titania glass. *J. Mater. Sci.* **28**, 177–183 (1993).
59. Kim, Y., Lee, S. & Yoon, H. Fire-safe polymer composites: flame-retardant effect of nanofillers. *Polym. (Basel).* **13**, 540 (2021).
60. Strongone, V. et al. Preparation and characterization of UV-LED curable acrylic films containing biochar and/or multiwalled carbon nanotubes: Effect of the filler loading on the rheological, thermal and optical properties. *Polym. (Basel).* **12**, 796 (2020).
61. ISO 2602:1980 (R.2021). Statistical interpretation of test results. International Organization for Standardization, Switzerland.
62. Gonçalves, F. A. M. M., Santos, M., Cernadas, T., Alves, P. & Ferreira, P. Influence of fillers on epoxy resins properties: a review. *J. Mater. Sci.* **57**, 15183–15212 (2022).
63. Reu, P. All about speckles: aliasing. *Exp. Tech.* **38**, 1–3 (2014).

Author contributions

Michele Perrella: Writing – original draft, Investigation, Formal analysis, Conceptualization, Supervision, Validation.Aurelio Bifulco: Writing – original draft, Investigation, Formal analysis, Conceptualization. Claudio Imparato: Writing – original draft, Investigation, Formal analysis. Immacolata Climaco: Visualization, Investigation, Formal analysis. Antonio Aronne: Writing – review & editing, Validation, Supervision.Mattia Bartoli: Investigation, Formal analysis.Matteo Bruno: Writing – original draft, Investigation.Gabriele Cricrì: Writing – review & editing, Validation.Enrico Armentani: Writing – review & editing, Validation, Supervision.

Funding

No funding was received for conducting this study.

Declarations

Competing interests

The authors declare no competing interests.

Additional information

Supplementary Information The online version contains supplementary material available at https://doi.org/10.1038/s41598-025-89963-5.

Correspondence and requests for materials should be addressed to M.P.

Reprints and permissions information is available at www.nature.com/reprints.

Publisher's note Springer Nature remains neutral with regard to jurisdictional claims in published maps and institutional affiliations.